Bio-Nanotechnology

Nonblinking Plasmonic Quantum Dot Assemblies for Multiplex Biological Detection**

*Fayi Song, Peter S. Tang, Holly Durst, David T. Cramb, and Warren C. W. Chan**

Optical labels enable visualization and detection of molecules, cells, and tissues. These labels have limited multiplexing capabilities, blink on/off at the single-molecule level, and, in many cases, they have low brightness. We address each of these issues through the development of a sub-50 nm barcoded optical label system by coating fluorescent quantum dots onto the surface of plasmonic nanoparticles using a layer-by-layer polyelectrolyte deposition strategy. We denote these gold nanoparticle–quantum dot hybrid structures as GQHs. This probe design strategy has the potential to create thousands of uniquely emitting nonblinking fluorescent probes. These barcodes can be further conjugated to biorecognition molecules, target cells, and have prolonged intracellular retention with minimal toxicity. Our results demonstrate that plasmonic nanoparticles are ideal templates for designing nanoscale barcodes.

Quantum dots are semiconductor nanocrystals with a broad excitation range and tunable emission spectra, enabling spectral multiplexing at a single excitation wavelength.[1,2] Their narrow and symmetric emission profile simplifies color discrimination.[3,4] Quantum dots are also brighter and more photostable than conventional organic fluorophores.[1] Quantum dots have been used as labels for staining diseased cells and tissues, single molecule analysis in live cells, and as contrast agents for in vivo cancer detection, but there is a need to increase the multiplexing capabilities of quantum dots to address the detection needs in biology and medicine.[5] Despite the size- and shape-tunable emission of quantum dots, a maximum of only seven different emitting quantum dots have been distinguished in cell experiments.[6]

To address this problem, researchers have started to encapsulate or dope quantum dots inside 200 nm to 10 μm polymer beads for protein or nucleic acid detection.[7] This detection platform has improved the efficiency and accuracy of molecular analysis and detection in vitro. The use of these barcodes for studying cells or molecules within cells is limited by their inefficient cellular uptake. Rejman and co-workers showed that 500 nm beads are taken up 8–10 times less efficiently than 50 nm beads.[8] Strategies have been attempted to encapsulate quantum dots inside sub-100 nm-sized beads, but it can be difficult to control the number and ratio of different emitting quantum dots inside nanometer-sized beads. Such limitation leads to inaccurate coding.

Size reduction of the barcode to the nanoscale is further constrained by the intrinsic fluorescence intermittency, or blinking behavior, of quantum dots. This property can complicate the acquisition, detection, and analysis of the emission from single quantum dots, as blinking may lead to false-negative signals. This blinking behavior is not a problem for microscale barcodes because they contain thousands of quantum dots loaded inside.[3] Suppression of blinking has been demonstrated by coupling quantum dots to plasmonic gold films[9] or by placing these particles near each other on a flat surface.[10] Plasmonic quantum dots have been recently developed with a quantum dot core encapsulated in a gold shell, but this design showed reduced fluorescence, and the blinking behavior was not characterized.[11] These plasmonic quantum dots may not be feasible for barcoding as each nanocomposite only contained a single quantum dot. Finally, non-blinking ZnSe capped CdZnSe quantum dots can be prepared by gradually alloying the Zn in the core, but their emission spectra is difficult to control.[12] We created nanobarcodes by using a layer-by-layer deposition strategy[13] to deposit a combination of quantum dots onto the surface of a gold nanoparticle. The gold nanoparticles enhanced the fluorescence and reduced the blinking of the quantum dots. The size of these hybrid structures is approximately 50 nm, which is small enough to enter cells and interact with biological molecules.[14]

To develop these nanobarcodes, gold nanoparticles were coated with different emitting quantum dots with a layer-by-layer polyelectrolyte deposition strategy. By carefully controlling the amount of the polyelectrolyte deposition, we were able to control the distance between the gold nanoparticles and quantum dots. It has been demonstrated that the maximum enhancement of quantum dot fluorescence can be achieved when the quantum dot is 11 nm away from the metal surface.[15] To obtain maximum fluorescence enhancement, citrate-coated gold nanoparticles were first coated with an amphiphilic diblock copolymer (polystyrene-*block*-poly(-

[*] Dr. F. Song, P. Tang, Prof. Dr. W. Chan
Institute of Biomaterials and Biomedical Engineering
Donnelly Centre for Cellular and Biomolecular Research
Chemical Engineering, Chemistry, Materials Science and
Engineering, University of Toronto
Toronto, ON, M5S 3G9 (Canada)
E-mail: warren.chan@utoronto.ca

H. Durst, Prof. Dr. D. Cramb
Department of Chemistry, University of Calgary
Calgary, AB, T2N 1N4 (Canada)

acrylic acid)).[16] An increase of about 5 nm in the radius of the nanoparticle can be measured by transmission electron microscopy. After centrifugal purification, the polymer-coated gold nanoparticles were coated with a second layer of positively charged poly(allylamine) polymer based on their electrostatic interaction. Caruso et al.[17] reported an increase of 1.2 nm after this addition. The shell thickness was controlled by repetitively alternating the negative and positive polymer coating. The gold nanoparticles with positively charged coating were functionalized with negatively charged quantum dots, resulting in plasmonic fluorescent nanoparticle hybrids. Figure 1a shows the nanobarcode design. Excess quantum dots were purified by repeated centrifugation. The developed layer-by-layer technique enabled facile manipulation of surface charges of gold nanoparticles, quantum dots, and their hybrids with polyelectrolytes. The purified nanobarcodes did not precipitate out of solution throughout storage in pure water, phosphate buffered saline, and medium with 10 % serum at 4 °C (Supporting Information, Figure S1).

Next, we demonstrated the deposition of different emitting quantum dots to the surface of the gold nanoparticles to create nanoscale barcodes. Figure 1b shows nanobarcodes composed of green and red quantum dots emitting at 525 nm and 665 nm, respectively. Different stoichiometric ratios of the green and red quantum dots were used in nanobarcode fabrication. Figure 1c shows pink light scattering of the fabricated nanobarcodes. This pink color is characteristic for dispersed gold nanoparticles in solution, in comparison to the purple/black color for their aggregates. Figure 1d,e demonstrate anticipated green to red fluorescence and spectral transition as the green-to-red quantum dot ratio decreased. Figure 1f shows optical images of the nanobarcodes using a single excitation wavelength. Such simultaneous excitation is not possible with conventional organic dyes. We show the coating of four different emitting quantum dots on the gold nanoparticle surface (Supporting Information, Figure S2). This fulfills the requirement for nanobarcoding application where multiplexing of more than two different quantum dots is achieved. We can also design these barcodes to emit in the near IR range, where cellular autofluorescence is low and tissue penetration is optimal (Supporting Information, Figure S2b).[18] We then demonstrated the multiplex biological detection application of these GQHs. Three different cell lines were first labeled with GQHs before being re-plated into the triple cell co-culture system. The three GQH-labeled cell lines were easily distinguished through fluorescence microscopy (Figure 1g).

Transmission electron micrograph images (Supporting Information, Figure S3) of monodisperse 15 nm citrate-stabilized gold nanoparticles and polymer-coated particles with narrow size variation showed a core diameter of (14.2 ± 1.2) nm and a polymer shell thickness of (9.2 ± 1.4) nm. Figure S3c shows a typical transmission electron micrograph image of the GQH ($\lambda_{em} = 600$ nm) with an average quantum dot-to-gold nanoparticle ratio of 4.17 ± 1.42. We were able to manipulate the number of quantum dots in the hybrid by adjusting the initial quantum dot-to-gold nanoparticle ratio, or using different sizes of gold nanoparticles. We increased
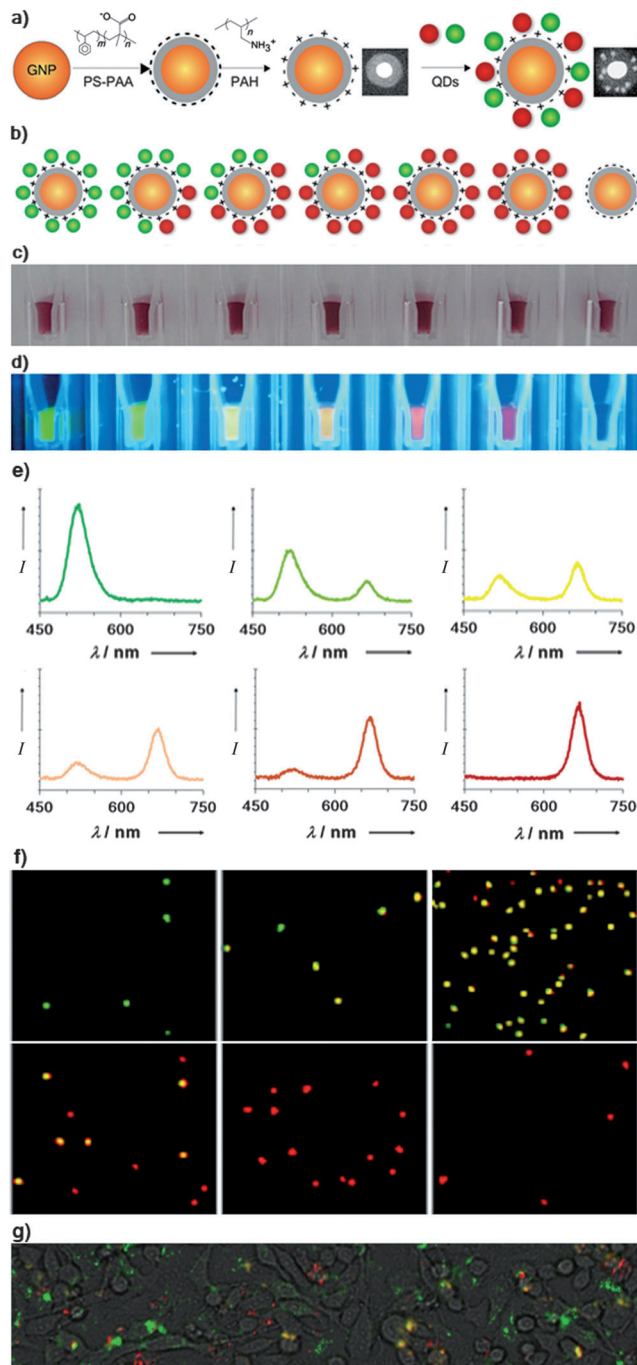

Figure 1. Gold nanoparticle–quantum dot barcodes. a) Preparation of gold nanoparticle–quantum dot hybrids (GQH). Insets: Representative transmission electron microscopy images of a polymer-coated gold nanoparticle and a GQH. Image height equals 50 nm. b) GQH nanobarcodes. The colorimetric and fluorescence properties of GQHs can be visualized under ambient light (c) and UV light (d). e) The fluorescence spectra for each of the GQHs. f) Fluorescence microscopy images of a single GQH. The images were first acquired separately with band-pass filters ($\lambda_{em} = 515/30$ and $\lambda_{em} = 650/50$) under a mercury lamp excitation ($\lambda_{ex} = 460/50$) and a 40× objective (NA = 0.85) before superimposition (ImageJ). Image height: 38 μm. g) Multiplex biological detection by GQHs. A549, HeLa, and Raw 264.7 cells were first labeled with GQH530 (green), GQH530-630 (yellow), and GQH630 (red), respectively, before being re-plated into a triple-cell co-culture system. Microscopy images were then acquired and superimposed similarly (as in f), except the band-pass filters ($\lambda_{em} = 530/10$ and $\lambda_{em} = 650/50$) and the objective (10×, NA = 0.30). Image height: 100 μm.

this ratio to 6.40 ± 1.53 and 8.00 ± 2.08 by using gold nanoparticles of 30 and 60 nm cores, respectively (Supporting Information, Figure S4a,b). Scanning electron micrograph images demonstrate that quantum dots reside on the surface of the hybrids (Supporting Information, Figure S4c,d). As the gold nanoparticles become smaller, the precision of placing a specific number of quantum dots on the surface decreases. However, the increased heterogeneity may not be critical for multiplex experiments as long as the optical signal can be discriminated from the GQHs. Using flow cytometry, we clearly demonstrate the ability to spectrally identify the GQHs (Supporting Information, Figure S5). This suggests that in any multiplex experiments using GQHs, the ability to spectrally identify the GQHs may need to be characterized prior to any multiplex application. We also wish to point that it is difficult to encapsulate quantum dots inside sub-50 nm polymeric beads. The smaller barcode size may be important for maximizing cellular uptake. An advantage of our strategy is the ability to engineer barcodes in this small nanometer size range that can maximize cellular uptake.

Figure 2. Enhanced quantum dot brightness with suppressed blinking. a) Fluorescence correlation spectroscopy autocorrelation decay of GQH600. Insert: quantum dots emitting at 600 nm without a gold core. The region at $\tau < 10^{-3}$ s contains information on blinking (see arrow). Note that there is no leveling off of the decay for the insert, indicating blinking. b) Normalized count-rate trajectories for nanoparticles containing 665 nm emitting quantum dots with (black) and without (red) a gold core. Note the large increase in brightness with the gold core. c) Fluorescence cross-correlation decay of gold nanoparticles coated with 600 nm and 665 nm emitting quantum dots. The large amplitude indicates nanoparticles containing both color quantum dots. d) Count-rate trajectories from 600 nm (red) and 665 nm (black) fluorescence channels observed for GQHs coated with both 600 and 665 nm quantum dots. The simultaneous events show both quantum dots are on the surface of the gold nanoparticles.

Absorbance and fluorescence spectra of the GQHs retained both plasmonic and fluorescent properties. Gold nanoparticles of 15 nm showed the characteristic plasmonic wavelength shift from 518 nm to 536 nm and 537 nm after deposition of the polymers and quantum dots, respectively (Supporting Information, Figure S6a). We did not observe an absorbance peak in the red wavelength that is typical for gold nanoparticle aggregation, indicating that these are single gold nanoparticles. Quantum dots alone and the GQHs showed virtually identical fluorescence spectra (Supporting Information, Figure S6b).

We next used single particle spectroscopy to determine whether there was a fluorescence enhancement and intermittence suppression of the quantum dots when they are placed on the surface of the gold nanoparticle. The nanoparticles were diluted into ultrapure water and examined using two-photon excitation fluorescence correlation spectroscopy (TPE-FCS).[19] We have previously demonstrated a connection between two-photon excitation saturation and blinking in quantum dots.[19] In the case of the single color
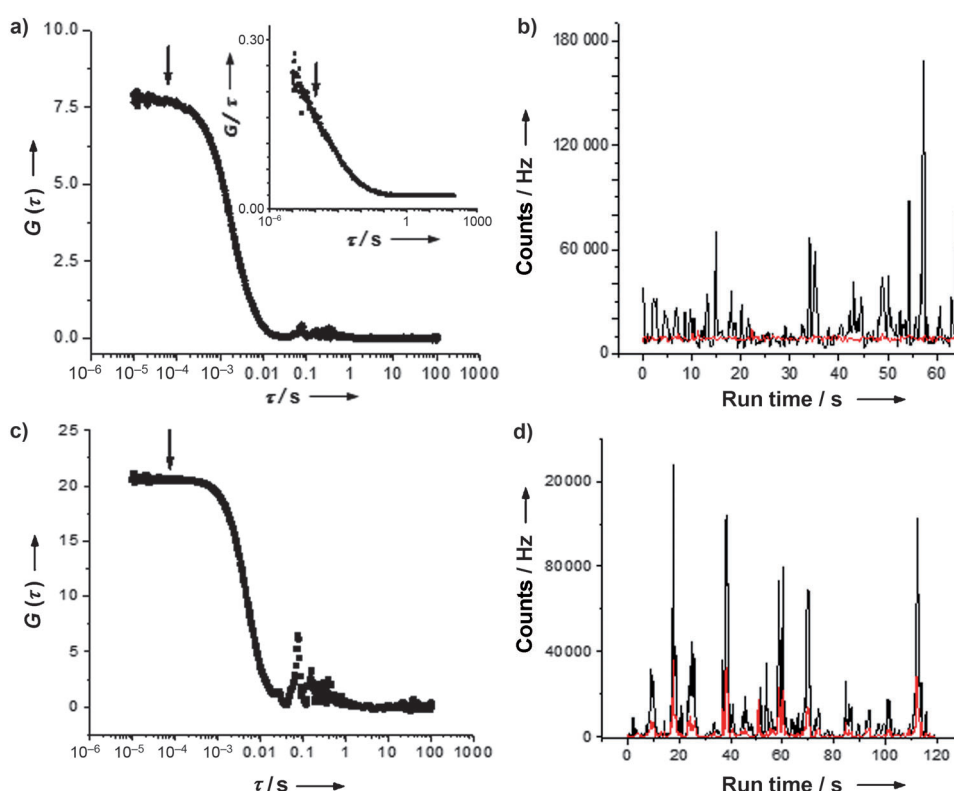
particles, autocorrelation decays were collected for GQH600 (Figure 2a). The insert of Figure 2a shows the autocorrelation decay for the P600 nanoparticles (without a gold nanoparticle core). This decay for P600 is typical of quantum dots displaying blinking dynamics, as they transit the two-photon excitation volume because it shows no apparent leveling off at short lagtime τ.[19] In comparison, the GQHs display a clear leveling of the autocorrelation decays at short τ, suggesting suppression of blinking. Additionally, the gold coating vastly increases the brightness of the nanoparticles. Figure 2b shows count rate trajectories for nanoparticles with 665 nm emitting quantum dots with and without a gold nanoparticle core. The trajectories are normalized to the count rate per particle. We determined the brightness η from the autocorrelation amplitudes (level region of autocorrelation decay, $G(0)$ values), and the average count rates CR_{av}. As $G(0)$ is equal to $1/N_{av}$, the relative brightness per particle can be determined ($\eta = G(0) \times CR_{av}$). For GQH600, $\eta = 20$ kHz/particle, and for GQH665, $\eta = 40$ kHz/particle, whereas for P600, $\eta = 11$ kHz/particle and for P665, $\eta = 8$ kHz/particle. Thus, at least a doubling in brightness was observed.

The nanoparticles with both 600 and 665 nm emitting quantum dots on the gold nanoparticle surface were analyzed

using a combination of FCS and fluorescence cross-correlation spectroscopy (FCCS).[20] Typical cross-correlation decay is shown in Figure 2c. Figure 2d shows a count rate trajectory for the two-color particles. The trajectory plot indicates many events occurring simultaneously in both detection channels. This is suggestive of nanoparticles that emit fluorescence of both colors. Confirmation comes in the large cross-correlation amplitude (Figure 2d).

We then demonstrated biological applications of these barcodes by modifying their surfaces for cellular uptake. It is well-known that positively charged particles and molecules enter cells spontaneously.[21] HeLa cells were treated for 24 h with positively or negatively charged quantum dots and GQHs. The positively charged GQHs showed superior intracellular fluorescence signals to their negatively charged counterpart, and positively and negatively charged quantum dots. The intracellular fluorescence of these positively charged hybrids was retained over three days, as demonstrated by confocal microscopy (Supporting Information, Figure S7) and flow cytometry (Figure 3a). These positively
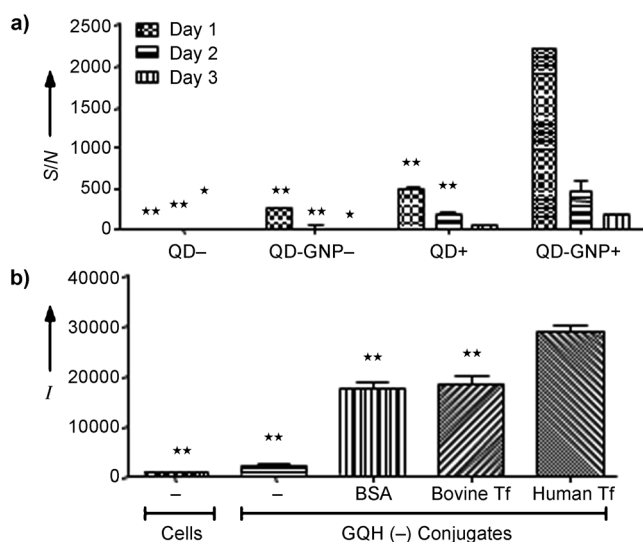

Figure 3. Cellular uptake of GQHs. a) Flow cytometry quantitatively showed significantly higher signal-to-noise ratio per cell (S/N) of positively charged GQHs (GQH+), which remained as high as around 200 on Day 3. b) Flow cytometry quantitatively showed significantly higher signals for the human transferrin (Tf)-conjugated GQH (−) in comparison to bovine Tf or bovine serum albumin (BSA). Error bars: standard deviation of two sample replicates with 1000 (a) or 10000 (b) cells each. * $p < 0.001$, ** $p < 0.05$ compared to GQH (+) of the same day (a) or to GQH (−) human Tf conjugates (b).

charged hybrids (GQH+) showed a four-fold higher uptake amount on Day 1, with a signal-to-noise ratio of 2200 compared to a value of 500 for the similarly positively charged quantum dots. The value remained as high as 200 for GQH(+) compared to a value of below 50 for the similarly positively charged quantum dots on Day 3, demonstrating the prolonged retention with high signal-to-noise ratios for GQH(+) inside cells. It is known that nanoparticle size and shape affects how much and how long a nanoparticle stays within a cell. Single quantum dots smaller than 6 nm can

rapidly exocytose out of some mammalian cells. By placing the quantum dots on the surface of the gold nanoparticle, the overall size increases, which increases the total number of quantum dots inside the cells. These GQHs are 52 and 260 times less toxic than CdTe and $CdCl_2$ based on comparison of the half maximal inhibitory concentrations (IC_{50}) of viability (Supporting Information, Figure S8). This is not surprising, as previous studies have shown that a ZnS shell mitigated cytotoxicity.[22]

Next, we examined whether these nanoscale barcodes can be conjugated to biological molecules and bind to cellular targets. Negatively charged nanobarcodes containing carboxylic acid groups were conjugated to the iron-transporting human or bovine protein transferrin or bovine serum albumin using carbodiimide chemistry. They were then incubated with HeLa cells. Successful conjugation was confirmed by a gel shift assay (Supporting Information, Figure S9) showing retarded migration of the protein-conjugated GQH compared with their unconjugated counterparts. Figure 3b shows that the human transferrin protein facilitated cellular uptake of the conjugated GQH by flow cytometry. This is also confirmed by wide-field and confocal fluorescence microscopy (Supporting Information, Figures S10, S11). Our cell line specifically expressed receptors for human transferrin. The cellular uptake is attributable to human transferrin receptor-mediated endocytosis, as demonstrated by a competition assay, in which excess human transferrin abolished the cellular uptake human transferrin-conjugated GQHs. Celluar uptake was noted for both bovine transferrin and bovine serum albumin-conjugated GQHs. However, such uptake was significantly less compared to their human transferrin-conjugated GQH counterpart. The increased cellular uptake likely attributed to the ligand–receptor specificity between human transferrin and its receptor on the human-derived HeLa cells.

In summary, we have developed the first nanobarcodes composed of gold nanoparticle cores and quantum dot encoded shells by layer-by-layer polyelectrolyte deposition. This technique enabled precise spatial control between quantum dots and plasmonic gold nanoparticles. Such control is critical for mediating fluorescence intermittence. The nanobarcodes preserved intrinsic optical and plasmonic properties of quantum dots and gold nanoparticles. These nanobarcodes were free of fluorescence intermittence and could be conjugated to biorecognition molecules for targeting applications. We demonstrate potential biological applications of these nanobarcodes to long-term cell tracking, which might be important in identifying stem cell differentiation and monitoring and detecting tumor metastasis. More importantly, our approach is simple and applicable to designing other types of multifunctional nanosystems.

[1] W. C. Chan, S. Nie, *Science* **1998**, *281*, 2016–2018.

[2] M. Bruchez, Jr.,, M. Moronne, P. Gin, S. Weiss, A. P. Alivisatos, *Science* **1998**, *281*, 2013–2016.

[3] M. Y. Han, X. H. Gao, J. Z. Su, S. Nie, *Nat. Biotechnol.* **2001**, *19*, 631–635.

[4] a) J. K. Jaiswal, H. Mattoussi, J. M. Mauro, S. M. Simon, *Nat. Biotechnol.* **2003**, *21*, 47–51; b) I. L. Medintz, H. T. Uyeda, E. R. Goldman, H. Mattoussi, *Nat. Mater.* **2005**, *4*, 435–446.

[5] J. M. Klostranec, Q. Xiang, G. A. Farcas, J. A. Lee, A. Rhee, E. I. Lafferty, S. D. Perrault, K. C. Kain, W. C. W. Chan, *Nano Lett.* **2007**, *7*, 2812–2818.

[6] P. K. Chattopadhyay, D. A. Price, T. F. Harper, M. R. Betts, J. Yu, E. Gostick, S. P. Perfetto, P. Goepfert, R. A. Koup, S. C. De Rosa, M. P. Bruchez, M. Roederer, *Nat. Med.* **2006**, *12*, 972–977.

[7] a) S. Fournier-Bidoz, T. L. Jennings, J. M. Klostranec, W. Fung, A. Rhee, D. Li, W. C. W. Chan, *Angew. Chem.* **2008**, *120*, 5659–5663; *Angew. Chem. Int. Ed.* **2008**, *47*, 5577–5581; b) Y. L. Gao, W. L. Stanford, W. C. W. Chan, *Small* **2011**, *7*, 137–146; c) P. P. Pillai, S. Reisewitz, H. Schroeder, C. M. Niemeyer, *Small* **2010**, *6*, 2130–2134.

[8] J. Rejman, V. Oberle, I. S. Zuhorn, D. Hoekstra, *Biochem. J.* **2004**, *377*, 159–169.

[9] X. W. Wu, M. Gong, C. H. Dong, J. M. Cui, Y. Yang, F. W. Sun, G. C. Guo, Z. F. Han, *Opt. Express* **2010**, *18*, 6340–6346.

[10] D. Ratchford, F. Shafiei, S. Kim, S. K. Gray, X. Q. Li, *Nano Lett.* **2011**, *11*, 1049–1054.

[11] Y. D. Jin, X. H. Gao, *Nat. Nanotechnol.* **2009**, *4*, 571–576.

[12] X. Y. Wang, X. F. Ren, K. Kahen, M. A. Hahn, M. Rajeswaran, S. Maccagnano-Zacher, J. Silcox, G. E. Cragg, A. L. Efros, T. D. Krauss, *Nature* **2009**, *459*, 686–689.

[13] a) G. Decher, *Science* **1997**, *277*, 1232–1237; b) F. Caruso, R. A. Caruso, H. Mohwald, *Science* **1998**, *282*, 1111–1114.

[14] a) B. D. Chithrani, A. A. Ghazani, W. C. W. Chan, *Nano Lett.* **2006**, *6*, 662–668; b) W. Jiang, B. Y. S. Kim, J. T. Rutka, W. C. W. Chan, *Nat. Nanotechnol.* **2008**, *3*, 145–150.

[15] O. Kulakovich, N. Strekal, A. Yaroshevich, S. Maskevich, S. Gaponenko, I. Nabiev, U. Woggon, M. Artemyev, *Nano Lett.* **2002**, *2*, 1449–1452.

[16] M. X. Yang, T. Chen, W. S. Lau, Y. Wang, Q. H. Tang, Y. H. Yang, H. Y. Chen, *Small* **2009**, *5*, 198–202.

[17] a) F. Caruso, *Adv. Mater.* **2001**, *13*, 11–22; b) F. Caruso, H. Lichtenfeld, E. Donath, H. Mohwald, *Macromolecules* **1999**, *32*, 2317–2328.

[18] S. Kim, Y. T. Lim, E. G. Soltesz, A. M. De Grand, J. Lee, A. Nakayama, J. A. Parker, T. Mihaljevic, R. G. Laurence, D. M. Dor, L. H. Cohn, M. G. Bawendi, J. V. Frangioni, *Nat. Biotechnol.* **2004**, *22*, 93–97.

[19] R. F. Heuff, M. Marrocco, D. T. Cramb, *J. Phys. Chem. C* **2007**, *111*, 18942–18949.

[20] a) K. G. Heinze, A. Koltermann, P. Schwille, *Proc. Natl. Acad. Sci. USA* **2000**, *97*, 10377–10382; b) T. T. Nguyen, J. L. Swift, M. C. Burger, D. T. Cramb, *J. Phys. Chem. B* **2009**, *113*, 10357–10366.

[21] a) S. Pujals, J. Fernandez-Carneado, C. Lopez-Iglesias, M. J. Kogan, E. Giralt, *Biochim. Biophys. Acta Biomembr.* **2006**, *1758*, 264–279; b) S. J. Tan, N. R. Jana, S. J. Gao, P. K. Patra, J. Y. Ying, *Chem. Mater.* **2010**, *22*, 2239–2247; c) L. Wasungu, D. Hoekstra, *J. Controlled Release* **2006**, *116*, 255–264.

[22] A. M. Derfus, W. C. W. Chan, S. N. Bhatia, *Nano Lett.* **2004**, *4*, 11–18.